

Supercritical Accretion Discs in Ultraluminous X-ray Sources and SS 433

Sergei Fabrika^{1,2*}, Yoshihiro Ueda³, Alexander Vinokurov¹, Olga Sholukhova¹, Megumi Shidatsu³

¹ Special Astrophysical Observatory, Russia

² Kazan Federal University, Russia

³ Kyoto University, Japan

The black hole mass and accretion rate in Ultraluminous X-ray sources (ULXs) in external galaxies, whose X-ray luminosities exceed those of the brightest black holes in our Galaxy by hundreds and thousands of times^{1,2}, is an unsolved problem. Here we report that all ULXs ever spectroscopically observed have about the same optical spectra apparently of WNL type (late nitrogen Wolf-Rayet stars) or LBV (luminous blue variables) in their hot state, which are very scarce stellar objects. We show that the spectra do not originate from WNL/LBV type donors but from very hot winds from the accretion discs with nearly normal hydrogen content, which have similar physical conditions as the stellar winds from these stars. The optical spectra are similar to that of SS 433, the only known supercritical accretor in our Galaxy³, although the ULX spectra indicate a higher wind temperature. Our results suggest that ULXs with X-ray luminosities of $\sim 10^{40}$ erg s⁻¹ must constitute a homogeneous class of objects, which most likely have supercritical accretion discs.

ULXs have luminosities exceeding the Eddington limit for a typical stellar-mass black hole^{1,2}, $\sim 2 \times 10^{39}$ erg s⁻¹. Despite their importance in understanding the origin of supermassive black holes that reside in most of present galaxies, several critical questions are still open. What black hole masses do the ULXs contain? Do they possess standard accretion discs? Do they belong to a homogeneous class of objects? The most popular models for the ULXs involve either intermediate mass black holes (IMBH, 10^3 – $10^4 M_\odot$) with standard accretion discs⁴ or stellar-mass black holes ($\sim 10 M_\odot$) accreting at super Eddington rates⁵. Except for transient ULXs, both scenarios require a donor with a high mass loss rate in a close binary (like a massive star and an AGB star), which means a short evolution stage.

While the X-ray properties of the ULXs are astonishing, it has been impossible, from the X-ray data alone, to distinguish even the main ULX models proposed. Optical spectroscopy may provide us with unique information on the ULXs. Because the ULX optical counterparts are very faint targets (~ 22 – 24 mag), however, very deep observations with the largest telescopes are required.

Using the Japanese 8.2m telescope Subaru, we have obtained highest-quality optical spectra of four nearest, bona fide ULXs that have unambiguous optical counterparts, single star-like objects — Holmberg II X-1, Holmberg IX X-1, NGC 4559 X-7, and NGC 5204 X-1. All details on the observations and data reduction can be found in Supplementary Section 1.

Fig. 1 shows the spectra of the ULX optical counterparts (the full range data are given in Supplementary Fig. 1). Main features in all the spectra are the bright He II $\lambda 4686$, hydrogen H α , and H β emission lines. The lines are obviously broad; the widths range from 500 to 1500 km s⁻¹. In some objects we detect broad He I $\lambda 6678$, 5876 emission lines. The spectra are very blue (Supplementary Fig. 1), in agreement with the photometric results⁶.

We reveal that the ULX spectra are similar to those of WNL stars, or extreme hot Of supergiants — transition stars, or those of LBVs in their compact hot states^{7–9}. All these are massive stars in neighboring evolutionary stages. This indicates the presence of hot outflow in the binary system: it could be a stellar wind from the donor, an irradiated surface of the accretion disc, or a powerful disc wind. The spectra are also similar to that of SS 433¹⁰, the only known supercritical accretor in our Galaxy, a close binary consisting of an A-type supergiant and a stellar-mass black hole. SS 433 apparently exhibits a WNL-type spectrum^{3,11} because the physical conditions of its disc wind may be similar to those of stellar winds from WNL stars. The impression of the spectral similarity is strengthened because the absolute visual magnitudes of both WNLs and SS 433 are in the same range as in the ULX counterparts^{6,12} (Fig. 2). Note that these WNLs are not WN 5–7 stars, whose spectra are well described with a pure-helium models¹², but LBV-like WN 9–11 stars, which contain up to 70 % hydrogen. Such spectra of high luminosities with prominent He II emission lines have never been observed from any stellar-mass black hole X-ray binaries except for SS 433 and those having WNL donors.

However, neither very hot WNL nor LBV examples exhibit such strong He II $\lambda 4686$ emission lines relative to the hydrogen lines. If the abundance of hydrogen in the ULX donors were two times smaller from the Solar value, then it could make the He/H ratio five times larger, as observed in these ULX spectra (Supplementary Table 1). This

contradicts with the non-enhancement of the He I and Pickering He II lines indicating nearly normal abundance of hydrogen. Hence, the wind in the ULXs must be even hotter and more highly ionized than stellar winds in WNL or LBV stars.

All the spectra of the ULXs we obtained are surprisingly similar to one another. The averaged width (FWHM) of the He II line and of $H\alpha$ are $\approx 870 \text{ km s}^{-1}$ and $\approx 1000 \text{ km s}^{-1}$, respectively. Strikingly, we find that almost all ULX counterparts ever spectroscopically observed exhibit spectra similar to those of WN 9-11 stars, particularly in their broad and strong He II emission, including NGC 5408 X-1, NGC 1313 X-2, M81 X-6, and M 101 ULX-1^{15–18}. In Fig. 3 we plot the He II and $H\alpha$ line widths of our four objects supplemented with NGC 5408 X-1, which has a simultaneous spectrum including both He II and $H\alpha$.

We study the spectra of the ULX counterparts in the He II diagram⁷, where the relation between the line width and equivalent width of the He II line is plotted (Supplementary Fig. 2). Here the line width represents the terminal velocity of a stellar wind, while the equivalent width reflects its photosphere temperature and mass loss rate. We also include hottest transition stars from O2If to WN7ha⁹, recorded LBV transitions⁸, and SS 433¹⁰. The ULXs and SS 433 occupy a region of the hottest transition stars O2If/WN5 – O3.5If/WN7 stars⁹. However, their behavior in the He II diagram is nothing like stars. They exhibit night-to-night variability both in the line width and equivalent width by a factor of 2–3. Variability in the radial velocity of the line is also detected with amplitudes ranging from 100 km s^{-1} in Holmberg IX to 350 km s^{-1} in NGC 5204 (Supplementary Fig. 3).

First, we can exclude the case where these ULXs actually have WNL donors and their stellar winds produce the observed optical spectra. Indeed, the rapid variability of the He II line-width is difficult to be explained, because the wind terminal velocity in stars is determined by the surface gravity. A more critical problem is that a WNL star means the wind-fed accretion regime, which is not effective¹⁸. To provide the observed X-ray luminosity, $L_X \sim 10^{40} \text{ erg s}^{-1}$, one needs an unrealistically powerful wind from the donor if the accretor is a stellar mass black hole. If the primary star were an intermediate mass black hole (IMBH), then the variability of the donor’s orbital velocity would be much greater than observed (see Supplementary Section 4 for details). Another obvious argument is the high-quality optical spectrum of NGC 7793 P13 indicating a B9Ia supergiant companion¹⁴, which itself cannot produce the He II emission line. Therefore, the He II line observed in NGC 7793 P13 must be formed in the second companion, namely, in a photoionized wind from the accretion disc (Supplementary Section 4).

We next consider a possibility that the He II line is formed in the standard accretion disc around a massive black hole. To produce lines in emission, a strong irradiation of the disc surface by the central source is required. The He II lines trace hotter regions located closer to the black hole than the hydrogen lines, and therefore the He II line width is expected to be notably larger than that of $H\alpha$ in a normal geometry. Indeed, broad He II and hydrogen emission lines from the self-irradiated disc are observed in Galactic stellar-mass black hole X-ray binaries in ourbursts, such as V404 Cyg¹⁹, GRO J1655–40^{20,21} and GX 339–4²². In all these cases, the He II emission lines are exactly broader than the hydrogen ones. These sources did not reach the supercritical regime; the most reliable determination of the distance toward V404 Cyg based on the

astrometric VLBI observations indicates that the luminosity was not super-Eddington during its famous 1989 outburst²³. We can interpret that their irradiated discs are not blocked by disc winds completely, and hence we observe the He II emission directly at the disc surface. By contrast, the ULX spectra show that the He II line is narrower than the H α (Fig. 3) line. It is impossible to explain this fact by irradiated discs unless exotic models are invoked.

We finally examine if the optical spectra of our ULXs can be explained by a supercritical accretion disc (SCAD) with a stellar-mass black hole. Indeed, the only known supercritical accretor SS 433 shows a similar optical spectrum to ours, which is produced by the disc wind from the SCAD³. In SS 433 the He II line is narrower than H α ^{10,24}. The same is valid in WNL stars and LBV in their hot state^{9,25}. This suggests that the He II and H α lines are formed in different parts of radiatively accelerated disc winds, where more ionized gas located closer to the source has smaller outflow velocities.

In Supplementary Table 1, we present the mean equivalent widths (relative fluxes) of main emission lines in the ULX spectra with respect to SS 433. While the line fluxes in all our ULXs are very similar, the indicated ionization degrees are higher than that of SS 433; the hydrogen and He I lines are ≈ 12 times weaker than those in SS 433, while the two observed He II lines are only two times weaker. These testify less dense but hotter disc winds than that in SS 433.

While the luminosity is proportional to the mass accretion rate in standard discs, it is expected to have a logarithmical dependence in SCADs^{26,5} (Supplementary Section 5), because the excess gas is expelled as a disc wind and the accreted gas is advected with the photon trapping, contributing little to the photon luminosity. Instead, the SCAD luminosity has the same order of the Eddington luminosity, $L_{\text{Edd}} \approx 1.5 \times 10^{39} m_{10} \text{ erg s}^{-1}$, where m_{10} is the black hole mass in units of 10 solar masses. The mass accretion rate can provide a factor of several in the logarithmic term. Besides that, the funnel in the SCAD wind will collimate the X-ray radiation to an observer also with a factor of a few when observed with an inclination angle smaller than 40–50 degrees²⁷. Thus, the apparent X-ray luminosity of an ULX with a stellar mass black hole may well be up to $\sim 10^{41} \text{ erg s}^{-1}$. The SCADs are able to account for the huge X-ray luminosities of the ULXs.

The UV and optical luminosity may strongly depend on the original mass accretion rate \dot{M}_0 , because these budgets are mainly produced by the reprocess of the strong irradiation from the SCAD's wind (the excess gas). Using simple relations for the SCADs, we find that the optical luminosity of the wind $L_V \propto \dot{M}_0^{9/4}$ and the wind temperature $T \propto \dot{M}_0^{-3/4}$ (see Supplementary Section 5 for more detail discussion). Accordingly, we find that the mass accretion rates in the ULXs listed in Fig. 2 may be by a factor of 1.5–6 smaller and their wind temperatures are by 1.4–4 times higher than those in SS 433. SCAD models can explain both the relative dimness of the ULXs in the optical band and higher ionization states of their disc winds than those of SS 433. Thus, we can interpret that SS 433 is intrinsically the same as ULXs but an extreme case with a particularly high mass accretion rate, which could explain the presence of its persistent jets.

References

1. Makishima, K. et al. The Nature of Ultraluminous Compact X-Ray Sources in Nearby Spiral Galaxies. *Astroph. J.* **535**, 632-643 (2000)
2. Feng, H. & Soria, R. Ultraluminous X-ray sources in the Chandra and XMM-Newton era. *New Astron. Rev.* **55**, 166-183 (2011)
3. Fabrika, S. The jets and supercritical accretion disc in SS 433. *Astroph. Space Phys. Rev.* **12**, 1-152 (2004)
4. Madau, P. & Rees, M. J. Massive Black Holes as Population III Remnants. *Astroph. J.* **551**, L27-L30 (2001)
5. Poutanen, J., Lipunova, G., Fabrika, S., Butkevich, A. G. & Abolmasov, P. Supercritically accreting stellar mass black holes as ultraluminous X-ray sources. *Mon. Not. R. Astr. Soc.* **377**, 1187-1194 (2007)
6. Tao, L., Feng, H., Grisé, F. & Kaaret, P. Compact Optical Counterparts of Ultraluminous X-Ray Sources. *Astrophys. J.* **737**, id. 81 (2011)
7. Crowther, P. A. & Smith, L. J. Fundamental parameters of Wolf-Rayet stars. VI. Large Magellanic Cloud WNL stars. *Astron. Astrophys.* **320**, 500-524 (1997)
8. Sholukhova, O. N., Fabrika, S. N., Zharova, A. V., Valeev, A. F. & Goranskij, V. P. Spectral variability of LBV star V 532 (Romano's star). *Astrophys. Bull.* **66**, 123-143 (2011)
9. Crowther, P. A. & Walborn, N. R. Spectral classification of O2-3.5 If*/WN5-7 stars. *Mon. Not. R. Astr. Soc.* **416**, 1311-1323 (2011)
10. Kubota, K. et al. Subaru And Gemini Observations Of SS 433: New Constraint On The Mass Of The Compact Object. *Astrophys. J.* **709**, 1374-1386 (2010)
11. Fuchs, Y., Koch Miramond, L. & Ábrahám, P. SS 433: a phenomenon imitating a Wolf-Rayet star. *Astron. Astrophys.* **445**, 1041-1052 (2006)
12. Hamann, W.-R. & Koesterke, L. The nitrogen spectra of Wolf-Rayet stars. A grid of models and its application to the Galactic WN sample. *Astron. Astrophys.* **333**, 251-263 (1998)
13. Vinokurov, A., Fabrika, S. & Atapin, K. Ultra-luminous X-ray sources as supercritical accretion discs: Spectral energy distributions. *Astrophys. Bull.* **68**,

139-153 (2013)

14. Motch, C., Pakull, M. W., Soria, R., Grisé, F. & Pietrzyski, G. A mass of less than 15 solar masses for the black hole in an ultraluminous X-ray source *Nature* **514**, 198201 (2014)

15. Cseh, D. et al. Towards a dynamical mass of the ultraluminous X-ray source NGC 5408 X-1. *Mon. Not. R. Astr. Soc.* **435**, 2896-2902 (2013)

16. Roberts, T. P. et al. (No) dynamical constraints on the mass of the black hole in two ULXs. *Astron. Nachr.* **332**, 398 (2011)

17. Bregman, J. N., Felberg, J. N., Seitzer, P. J., Liu, J. & Kümmel, M. Ultraviolet Spectra of ULX Systems. ArXiv e-prints arXiv:1205.0424 (2012)

18. Liu, J., Bregman, J. N., Bai, Y., Justham, S. & Crowther, P. Puzzling accretion onto a black hole in the ultraluminous X-ray source M101 ULX-1. *Nature*, **503**, 500-503 (2013)

19. Charles P. A. et al. The bright X ray transient GS2023+338 (=V404 Cyg) in optical outburst and decline. *ESASP*, **296**, 103-107 (1989)

20. Hunstead R. W., Wu K., Campbell-Wilson D. New Radio and Optical Data for GRO J1655-40. *ASPC*, **121**, 63-67 (1997)

21. Soria, R., Wickramasinghe, D. T., Hunstead, R. W. Wu, K. Measuring the Motion of the Black Hole in GRO J1655-40. *Astrophys. J.* **495**, L95-L98 (1998)

22 Soria, R., Wu, K. Johnston, H. M. Optical spectroscopy of GX 339-4 during the high-soft and low-hard states - I. *Mon. Not. R. Astr. Soc.* **310**, 71-77 (1999)

23. Miller-Jones J. C. A. et al. The First Accurate Parallax Distance to a Black Hole. *Astrophys. J.* **706**, L230-L234 (2009)

24. Grandi, S. A. Stone, R. P. S. SS 433 - How the moving lines move. *Publ. Astron. Soc. Pacific* **94**, 80-86 (1982)

25. Walborn, N. R. Fitzpatrick, E. L. The OB Zoo: A Digital Atlas of Peculiar Spectra. *Publ. Astron. Soc. Pacific* **112**, 50-64 (2000)

26. Shakura, N. I. Sunyaev, R. A. *Astron. Astrophys.* Black holes in binary systems. Observational appearance. **24**, 337-355 (1973)

27. Ohsuga, K. & Mineshige, S. Global Structure of Three Distinct Accretion Flows and Outflows around Black Holes from Two-dimensional Radiation-

magnetohydrodynamic Simulations. *Astroph. J.* **736**, id. 2 (2011)

Acknowledgements

The authors are grateful to V. Shimansky, D. Nogami for helpful comments, and T. Hattori for his support in our observations. The research was supported by the Russian RFBR grant 13-02-00885, the Program for Leading Scientific Schools of Russia N 2043.2014.2, the Russian Scientific Foundation (grant N 14-50-00043) and the JSPS KAKENHI Grant number 26400228. S.F. acknowledges support of the Russian Government Program of Competitive Growth of Kazan Federal University. Based on data collected at Subaru Telescope, which is operated by the National Astronomical Observatory of Japan and on data obtained from the ESO Science Archive Facility (NGC 5408 X-1, ID 385.D-0782).

Author contributions S.F. and Y.U. proposed the observations and wrote the paper with comments from all authors. The observations were carried out by S.F., Y.U. and M.S. A.V. and O.S. prepared the observational details and reduced the data. S.F., Y.U. and A.V. discussed the results and overall science case with contribution from the remaining authors.

Author contributions The authors declare no competing financial interests. All correspondence should be addressed to S. Fabrika (email: fabrika@sao.ru)

Figure 1: Spectra of the ULX optical counterparts from top to bottom, Holmberg II, Holmberg IX, NGC 4559, and NGC 5204 in blue **(a)** and red **(b)** spectral regions. The spectra are normalized for better inspection. The most strong are the He II $\lambda 4686$ line and the hydrogen lines $H\alpha$ $\lambda 6563$ and $H\beta$ $\lambda 4861$. The broad He I $\lambda 6678$ line is also detected. Narrow nebular emission in $H\beta$ and [O III] $\lambda\lambda 4959, 5007$ lines is oversubtracted in two bottom spectra. Although the hydrogen lines are contaminated with the nebular emission, their broad wings are clearly seen.

Figure 2: Absolute magnitudes of all well-studied ULXs: Holmberg IX X-1, NGC 5204 X-1, NGC 4559 X-7, IC 342 X-1, NGC 5408 X-1, M 81 X-6, M 101 ULX-1, Holmberg II X-1, NGC 6946 ULX-1, NGC 1313 X-1, X-2)⁶ and SS 433 (shadowed) with some updates in the distances in the last four ULXs¹³ and NGC 7793 P13¹⁴.

Figure 3: Emission line widths of He II and $H\alpha$ of Holmberg II X-1, NGC 4559 X-7, NGC 5408 X-1, Holmberg IX X-1, and NGC 5204 X-1, from left to right, all extracted from simultaneous spectra. Systematic errors are taken into account in the error bars of $H\alpha$ because of the nebula line subtraction. The error on the He II line-width of NGC 5204 X-1 is large because of its fainter flux. Note that the averaged He II line width of NGC 1313 X-2 is 580 km/s¹⁶ measured in the spectra without $H\alpha$.

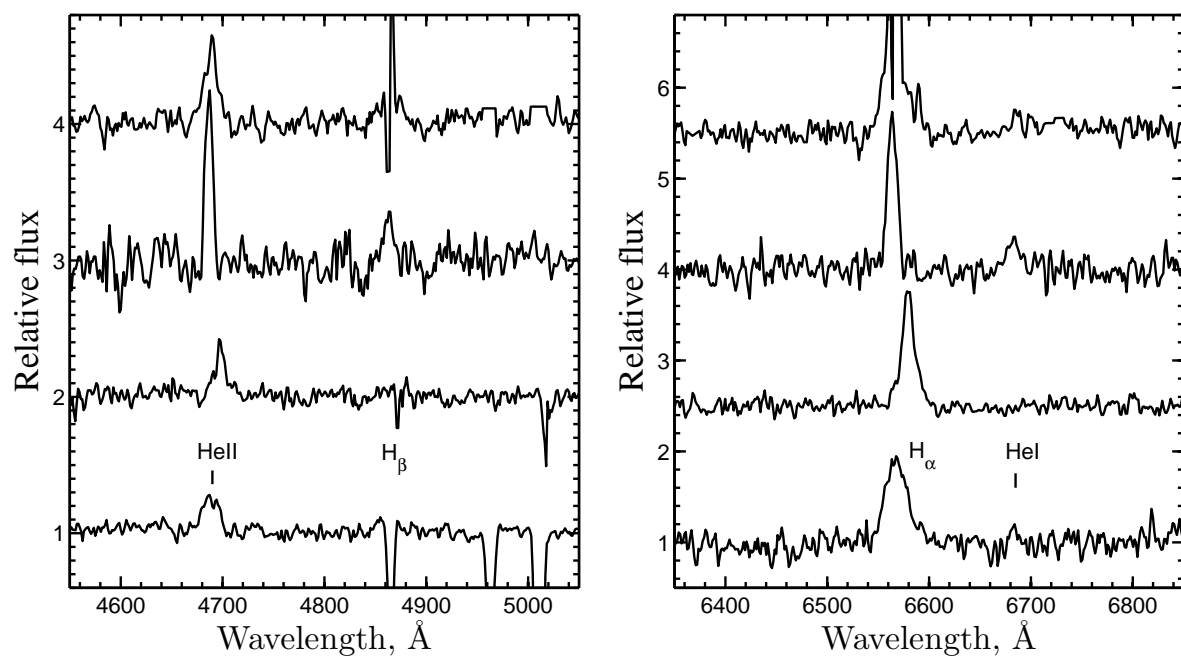


Figure 1:

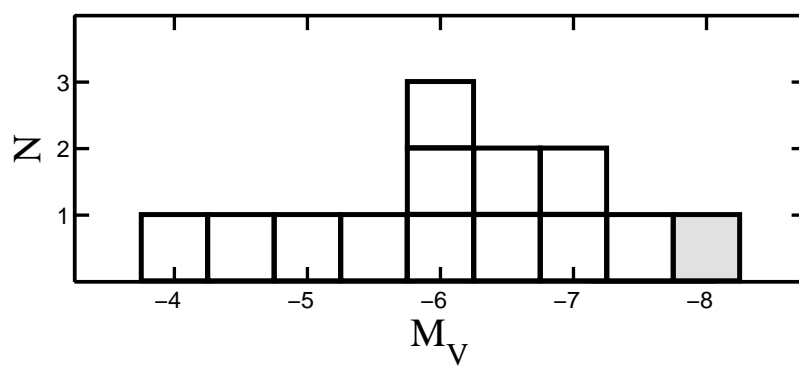


Figure 2:

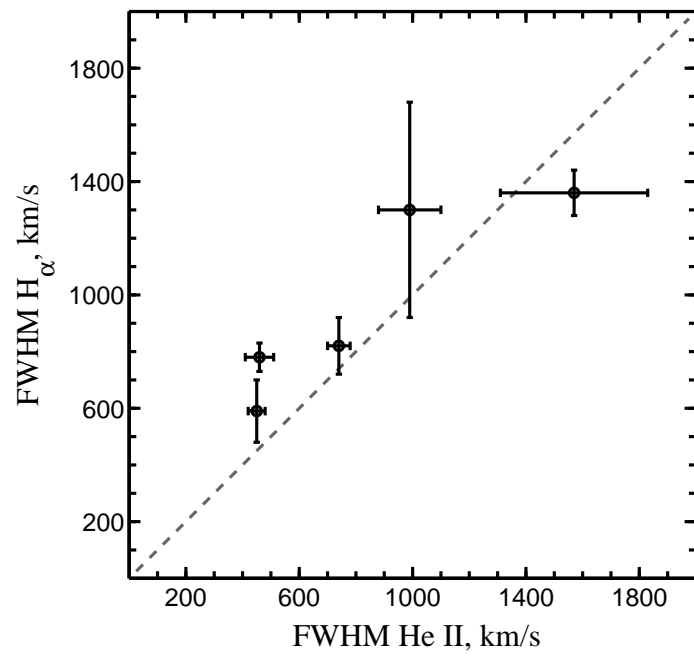


Figure 3:

Supplementary

The Supplementary part provides details on the Subaru spectroscopic observations, data reduction, spectral classification of the observed spectra, comparison of the spectra with those of SS 433, and interpretation of the results.

1 Observations

We observed ULX counterparts on 2011 February 25–28 with the Faint Object Camera and Spectrograph (FOCAS)²⁸, installed at the Cassegrain focus of the Subaru telescope. FOCAS was operated with the 300B grism without filter, providing a higher efficiency with a spectral range of 3650–8300 Å. The range was limited by scattered-light contamination at shorter wavelengths and by the order overlap at longer ones. Thus, the 3800 – 7000 Å range was used. Depending on seeing conditions, we used 0.4–0.8 arcsec slits, providing a spectral resolution of 1000 – 500, respectively. The seeing was ≈ 1.1 arcsec on the first night, continuously improving to 0.4–0.6 arcsec on the last night.

Our ULX targets are very faint, $V = 21.5, 22.0, 23.0$, and 22.5 in Holmberg II, Holmberg IX, NGC 4559, and NGC 5204, respectively^{6,29–32}. We tried to observe each target in each night to search for possible spectral and photometrical variability. With the exception of the first night when we observed only one target (in Holmberg II), the sky condition was mostly photometric. In total we obtained the net exposure of 280, 260, 300, and 320 minutes for the targets in Holmberg II, Holmberg IX, NGC 4559, and NGC 5204, respectively.

The data reduction was performed in a standard manner. Using Th–Ar lamp, we achieve the wavelength calibration accuracy better than 10 km s^{-1} in each spectra. However, because of the different instrumental flexure between the arc calibration spectra, the accuracy was degrading. We estimate a final accuracy in the night sum spectra as 15 km s^{-1} . The flux calibration is made by using standard stars observed every night.

The spectra extraction was not simple due to the nebular emission that surrounds almost all the ULX counterparts. We extracted the spectra with Gauss-profile aperture, and made two versions of the spectra. In the first one, we used extended regions of 4–10 arcsec for the background. Although this gives a higher S/N in the final spectra, the hydrogen lines originating from the nebulae may strongly contaminate the ULX spectrum. In the second version, we used very small regions for the background, ≈ 1 arcsec, and produced the spectra with the least contamination by the nebular lines. The last version was used mainly for measurements of hydrogen lines.

The reduced spectra are given in Supplementary Fig. 1. For Holmberg IX, we used the small regions for the background, while for NGC 4559 and NGC 5204, we used the extended regions. For Holmberg II, where a very bright nebula is concentrated at the central part, we used an intermediate aperture for the background. In Fig. 1, we show the spectra with the small apertures for the upper three targets. The different apertures are adopted for Holmberg II and NGC 4559 to obtain better insight how the nebulae may distort the final spectra.

2 Optical Spectra

We produced the normalized spectra for better inspection of spectral features (Fig. 1). The main feature in all the spectra is a broad He II $\lambda 4686$ emission line. The most narrow one is found from Holmberg IX, with an FWHM $\approx 450 \text{ km s}^{-1}$, and the most broad one is from NGC 5204, with an FWHM $\approx 1570 \text{ km s}^{-1}$ (all line widths are corrected for the spectral resolution). Note that the relatively narrow line in Holmberg IX is notably broader than any nebular emission and it is not contaminated with nebular He II emission.

Previously, optical spectra have been obtained for M 101 ULX-1, Holmberg IX X-1, NGC 5204 X-1, NGC 1313 X-2, NGC 5408 X-1, NGC 7793 P13^{14,16,18,33,34}. In all these targets the He II $\lambda 4686$ emission has been detected. There was one exception, NGC 5204 X-1, but we confidently detect the He II line from this ULX with our new data.

We conclude that all ULX counterparts ever spectrally observed have the same feature in their spectra, that is, a broad He II emission line. We also clearly detect broad H α , H β lines and He I $\lambda 6678$, $\lambda 5876$ lines (Supplementary Fig. 1). There is also some hints on the Bowen C III/N III blend (4640 - 4650 Å). Although the H β line is affected by nebular emission in spite of our careful extraction, its broad wings are clearly detected. It is obvious that the emission lines are formed in stellar winds or disc winds.

Since all the spectra of the ULX counterparts are very similar to one another, we analyze the mean parameters of the lines. We find that the average line width of H α is broader than that of He II, FWHM(He II)/FWHM(H α) ≈ 0.8 . We confirm that there is a good linear correlation between the He II and H α line widths in each object. The distributions of the observed line widths are plotted in Fig. 2.

We find that the gas where the lines are formed is very hot, because EW(He II)/EW(H β) ≈ 2.2 , EW(He II)/EW(H α) ≈ 0.36 , and EW(He II)/EW(He I $\lambda 5876$) $\gtrsim 3.6$. The hydrogen abundance is nearly normal in the winds, because the Pickering series are weak, EW(He II $\lambda 5411$)/EW(H β) $\lesssim 0.27$ (Supplementary Table 1). We note that EW of the H β line may be uncertain because of subtraction of nearby nebulae components, especially in NGC 4559 and NGC 5204. The H α line is measured with much better accuracy.

We detect a strong radial velocity variability of the He II $\lambda 4686$ line from night to night (Supplementary Fig. 3). We have not enough data to study orbital variability, however, it was not possible to obtain dynamical mass constraints in previous spectra^{15,16,35}. The He II line is free from contamination by the nebular He II emission in the three ULXs except in Holmberg II. This means that the radial velocity variability of the line is real. The line changes not only its position but also its intensity and width. In Supplementary Fig. 2 we show the line variability in EWs and FWHMs from night to night. An accuracy depends on the He II profiles. It is less than 0.5 Å (EW) and 30 km/s (FWHM) in the most regular lines of Holmberg IX X-1, and it is up to 1.5 Å and 250 km/s in structured He II lines in NGC 5204 X-1 (Fig. 1).

3 What the Spectra Resemble?

Among stellar spectra, such a strong He II line with a nearly normal hydrogen abundance can be found only in stars recently classified as O2–3.5If*/WN5–7⁹. We omit index * hereafter, which means a stronger ionization as indicated by N IV/N V lines. They are the hottest transition stars, whose classification is based on the H β profile, tracing the increasing wind density (i.e., the mass loss rate) from O2–3.5If to O2–3.5If/WN5–7, and to WN5–7. In Supplementary Fig. 2, we show the classification diagram of WN stars⁷ for LMC and Galactic objects. We supplement the diagram with additional stars recently classified⁹. The diagram plots stars in accordance with their wind velocity (FWHM) versus the photosphere temperature and mass loss rate (EW). Three known LBV transitions (LBV – WNL) between their hot and cool states in AG Car, V 532 in M 33, and HD 5980 in SMC are also shown in the figure. Consequent states in each LBV transition are connected with the lines. In their hotter state where the He II line becomes stronger, the LBVs fit well the classical WNL stars⁸.

We see that the ULX counterparts occupy a region at the He II diagram between O2–3.5If and WN5–7 (Supplementary Fig. 2). This is also a region of “intermediate temperature LBV” V 532 and the “LBV excursion” of HD 5980. However, their behavior in the diagram is nothing like stars. The variability of the He II lines of our counterparts in three consequent nights is shown by the points connected by the lines. If the ULX counterpart spectra were produced from donor stars, variable surface gravity at about the same photospheric temperature would be required. Instead, the spectra may be formed in unstable and variable winds formed in accretion discs. This idea agrees with the fact that we do not find any regularities between the EW, FWHM, and radial velocity of the He II line.

In the figure, we also present two recently discovered extragalactic black holes NGC 300 X-1³⁶ and IC 10 X-1³⁷ together with the soft ULX transient M 101 ULX-1. The black holes in NGC 300 X-1 and IC 10 have luminosities $L_X \sim 3 \times 10^{38} \text{ erg s}^{-1}$, about the same as that of Cyg X-3, which certainly contains a WN-type donor star³⁸.

The same may be proposed for the transient source M 101 ULX-1 on the basis of its location in the diagram. It has been recently found that this source indeed contains a WN8 type donor¹⁸, although its orbital period is ~ 40 times longer than in Cyg X-3 and ~ 6 times longer than in two other WR X-ray binaries. This may be the reason for the difference of M 101 ULX-1 from the other WR X-ray binaries, i.e., its transient nature. Because of the large size of the Roche lobe around the compact star, the accretion disc is likely to be formed with a partial ionization zone¹⁸. In steady states, M 101 ULX-1 has a luminosity of an order of magnitude smaller than that of the Cyg X-3-type objects, although in an outburst peak the luminosity becomes an order of magnitude larger, close to the low boundary of the ULXs luminosity range.

The X-ray luminosities comparable with that of Cyg X-3, which are in line with the wind accretion and the short orbital periods, the location in the He II diagram, the detail analysis of optical spectra of the WR X-ray binaries^{36,37,18} confirm that their optical spectra come from WNL donors.

The only known supercritical accretor in our Galaxy SS 433 seems to be the most close relative to the ULXs. It has been proposed³ that SS 433 supercritical disc’s funnel will appear as an extremely bright X-ray source when observed in a nearly face-on geometry. The intrinsic luminosity of SS 433 (mainly in UV) is $\sim 10^{40} \text{ erg s}^{-1}$ and

all this budget is formed in the disc³. Nevertheless, the X-ray luminosity of SS 433 is not high, $\sim 10^{36}$ erg s⁻¹, because the emission is blocked by the thick accretion disc observed nearly edge-on. If one has a chance to observe the whole funnel, one may discover all the bolometric radiation in X-rays. Apparent X-ray luminosity of the face-on SS 433 is expected to be even larger than its bolometric luminosity, because of geometrical collimation in the funnel with a factor of $B = 2\pi/\Omega_f \sim 3 - 5$, where Ω_f is the solid angle of the funnel. The existence of SS 433 demands forthcoming X-ray sources with luminosities of a few $\times 10^{40}$ erg s⁻¹.

SS 433 in Supplementary Fig. 2 diagram nearly meets the ULX region. However, the ULX winds are notably hotter than the SS 433 wind. Comparing the ULX spectra with that of SS 433¹⁰ taken with the same instrument, we find that the average EWs of H α , H β , and He I $\lambda 5876$ lines in the ULXs are exactly ≈ 12 times smaller than those in SS 433, whereas the EWs of two He II lines ($\lambda\lambda 4686, 5412$) are only 2.2 times smaller than in SS 433 (Supplementary Table 1). We conclude that the ULX winds are not such powerful, but notably hotter, than that in SS 433. That is because their EWs are smaller and their He II/He I ratios are bigger than that in SS 433. In this sense, SS 433 remains the unique object. Indeed, the presence of the persistent jets in SS 433 may be explained by its extremely large mass accretion rate.

Below we discuss possible interpretations of the ULX optical spectra: a donor star and a supercritical discs with a stellar-mass black hole.

4 Are the ULX Spectra of the Donor Stars?

If the optical spectrum is formed in the donor star of WNL type, the He II line widths indicate the stellar wind velocity. We adopt this value as $V_W = 900 v_{900}$ km s⁻¹, where v_{900} is the wind velocity normalized by 900 km s⁻¹. The wind must supply a mass accretion rate \dot{M}_X to provide the observed X-ray luminosity of $L_X \sim 10^{40}$ erg s⁻¹. If we adopt an accretion efficiency $\eta = L_X/\dot{M}_X c^2 = 0.1$, we need $\dot{M}_X \sim 1.8 \times 10^{-6} M_\odot \text{ y}^{-1}$. Note this is the super-Eddington rate for black holes with masses smaller than 60 M_\odot . Both the mass accretion rate and black hole mass must be regarded as the lower limits because of advection of heat and radiation²⁷.

In the close binary consisting of a black hole and a WN star, the donor's mass loss rate in the wind must be $\dot{M}_{WN} = \dot{M}_X 4\pi a^2 / \pi R_c^2$, where a is the binary separation, $R_c \approx GM_{BH} / (V_W^2 + V_{orb}^2)^{1/2}$ is the capture (Bondi) radius and V_{orb} is the relative orbital velocity of the companion. Adopting the mass ratio in the binary as $q = M_{WN}/M_{BH} = 2$ and using Kepler's law, we find $\dot{M}_{WN} \approx 300 \dot{M}_X (p_1/m_{10})^{4/3} v_{900}^4 \approx 5 \times 10^{-4} M_\odot \text{ y}^{-1}$, where p_1 and m_{10} are the orbital period and black hole mass in units of 1 day and 10 M_\odot , respectively. Even for such a short period the donor's mass loss is too large for WNL stars³⁹. It is because the wind-fed accretion is not effective. The orbital velocity of the donor in the binary will be ~ 220 km s⁻¹. If one assumes smaller orbital periods or larger black hole masses, one finds higher orbital velocities, which are not observed in our observations (Supplementary Fig. 3).

There is an exotic case of the IMBH + WN donor binary ($M_{BH} \gg 10 M_\odot$, $V_{orb} \gg V_W$), where practically all the donor's wind is accreted by the black hole and hence $\dot{M}_{WN}/\dot{M}_X = 4(1 + q)^2$. Such a system can provide the observed X-ray luminosity of

$\sim 10^{40}$ erg s $^{-1}$. However, the donor's orbital velocity variations must be much larger than observed value, $V_{\text{orb}} \sim 2100(m_{1000}/p_1)^{1/3}$ km s $^{-1}$. We thus conclude that a WN donor cannot provide the ULX-like luminosity with a black hole of any masses. Indeed, three known examples of the short period binaries with WN donors, Cyg X-3, IC 10 X-1, and NGC 300 X-1, are not ULXs, which are ~ 30 times fainter in X-rays.

One finds a strong argument that the He II emission in the ULXs cannot be formed on a donor star. It comes from high-quality optical spectra of NGC 7793 P13, where the donor temperature of 11000 ± 1000 K has been measured¹⁴. We have studied the P13 spectra and confirm that neither the emission line EW nor the absorption spectrum of the B9Ia supergiant companion depends on the X-ray luminosity or the orbital phase of the system. We suggest that this object is somewhat different from the other ULXs, and hence additional studies are needed to completely understand its nature. Note that P13 is not a persistent ULX, whose X-ray luminosity is variable by a factor of 100, although it could be related to the source occultation by the disc.

5 Supercritical Discs with Stellar-Mass Black Holes

We have shown that the He II line is most likely formed in super-Eddington accretion discs with stellar-mass black holes. The supercritical regime has been first described by Shakura and Sunyaev²⁶. They introduced a “spherization radius” in the disc, $R_{\text{sp}} \propto \dot{M}_0$. The disc is standard at $r > R_{\text{sp}}$, while it becomes a supercritical one at all radii smaller than this point. The SCAD is geometrically thick with strong mass loss. The local mass accretion rate at $r < R_{\text{sp}}$ is Eddington limited, $\dot{M}(r) \sim \dot{M}_0 r / R_{\text{sp}}$. As the result, a strong disc wind inevitably appears in the supercritical region⁵. In recent 2D RHD simulations²⁷, which take into account both heat advection and photon trapping, the main ideas of the Shakura–Sunyaev’s SCAD approach have been confirmed.

In standard accretion discs, the bolometric luminosity is scaled with the mass accretion rate as $L \propto \dot{M}_0$, whereas, in SCADs, the luminosity depends on black hole mass and is nearly independent of mass accretion rate as $L \propto L_{\text{Edd}}(1 + a \ln(\dot{M}_0/\dot{M}_{\text{Edd}})) \propto M_{\text{BH}}^{26}$, where L_{Edd} and \dot{M}_{Edd} are the Eddington limit and corresponding mass accretion rate, respectively, and $a \sim 0.5 - 0.7$ is the parameter accounting for advection⁵. There are two more differences in SCADs from standard discs, (i) the X-ray radiation is geometrically collimated ($2\pi/\Omega_f$) in the wind funnel, and (ii) the UV/optical luminosity does depend stronger on the mass accretion rate than it is in a standard disc. In the SCAD all the gas in excess of the critical accretion rate is expelled as a disc wind¹³, which reprocesses the disc X-ray radiation. The wind forms a funnel whose size is nearly proportional to the mass accretion rate. This issue may resolve the dimness of the ULX optical counterparts with respect to SS 433 (Fig. 2).

The wind velocity V is expected to be virial at the spherization radius²⁶, $V \propto M_{\text{BH}}^{1/2} R_{\text{sp}}^{-1/2}$. The wind photosphere radius is given as $R_{\text{ph}} \propto \dot{M}_0 V^{-1} \propto \dot{M}_0^{3/2} M_{\text{BH}}^{-1/2}$ ³. The SCAD luminosity, $L \propto M_{\text{BH}} \propto R_{\text{ph}}^2 T^4$, is partially radiated at the wind photosphere. Combining these dependences, we find the photosphere temperature dependence as $T_{\text{ph}} \propto \dot{M}_0^{-3/4} M_{\text{BH}}^{1/2}$. In the optical Rayleigh–Jeans region, the luminosity is expressed as $L_V \propto R_{\text{ph}}^2 T \propto \dot{M}_0^{9/4} M_{\text{BH}}^{-1/2}$. Hence, the optical luminosity of the SCAD may strongly depend on the mass accretion rate.

In the picture described by Shakura-Sunyaev²⁶ the excess gas is ejected from the spherization radius R_{sp} at a virial velocity. This scale is estimated as $R_{\text{sp}} \sim \frac{\kappa \dot{M}_0}{8\pi c}$, where $\kappa = 0.34 \text{ cm}^2 \text{ g}^{-1}$ is the Thomson's opacity. In SS 433 one finds $R_{\text{sp}} \sim 3 \times 10^9 \text{ cm}$, and the corresponding virial velocity is $V \sim 9400 \text{ km s}^{-1}$. The velocity is one magnitude bigger than that observed in SS 433 and in the ULX counterparts. It is possible, however, that the actual situation is much more complex than the simplified picture that the gas is directly ejected without any interactions in the wind. To account for the discrepancy between the predicted velocity and observed ones, it is suggested, in modelling of the SS 433 wind⁴⁰, that the escaping gas is mixing because of effective mass loading of the funnel region. Also, it is known from hydrodynamic simulations^{41,27} that some portions of the gas are launched at velocities less than the virial one and return to the disc, but the excess gas eventually leaves the disc.

Note that the gas ejected at R_{sp} is optically thick in continuum. The process occurs very deeply under the photosphere, R_{ph} , whose size is about three orders of magnitude larger than the launching radius. At $R > R_{\text{ph}}$, the gas remains to be optically thick in lines. That is a principal difference between supercritical disc outflows and WNL/LBV winds; in supercritical discs, the gas is launched in very inner regions. Above the photosphere, however, the winds may behave about the same way.

We cannot know all acceleration processes in disc winds without detailed modelling up to the photosphere size. If we assume that the gas velocity is constant, we find $R_{\text{ph}} \propto \dot{M}_0$, $T_{\text{ph}} \propto \dot{M}_0^{-1/2} M_{\text{BH}}^{1/4}$, and $L_V \propto \dot{M}_0^{3/2} M_{\text{BH}}^{1/4}$. Indeed, estimates of these values are based on the velocity around the photosphere, where the gas velocity cannot change rapidly. In such a case, we again see that the optical luminosity of the winds does depend notably on the gas accretion rate.

At supercritical accretion rates ($\dot{M}_0 > \dot{M}_{\text{Edd}}$), the extended photosphere of the wind hides its formation region, and hence $R_{\text{ph}} > R_{\text{sp}}$, where R_{ph} is the location of the photosphere. It is known that in SS 433, $\dot{M}_0 \gg \dot{M}_{\text{Edd}}$ ³. It is the brightest object in the V -band among all studied ULX counterparts (Fig. 2), by a factor from 2 to 60. Using the scaling relations derived above ($L_V \propto \dot{M}_0^{9/4}$), we find that the mass accretion rates in the ULXs are smaller than that in SS 433 by a factor from 1.5 to 6 and their wind temperatures are higher by 1.4–4. SS 433 wind has a temperature of $\sim 50 \text{ kK}$ ³ in its precession phase where the disc is the most open to the observer. We thus estimate the wind temperatures in the ULXs to be 70–200 kK. (If we take another scaling relation, $L_V \propto \dot{M}_0^{3/2}$, we find that in the ULXs the mass accretion rates are smaller by a factor of 1.6 – 15, while the wind temperatures are higher by the same factor, 1.4–4, compared with SS 433).

The ULX winds are very hot, because they are directly heated by the strong X-ray radiation. Thus, the simple SCAD model may explain both the relative dimness of the ULX counterparts in the optical bands as well as the higher ionization stage of the winds than in SS 433. The He II and H α lines are produced in outer parts of the wind, not in the wind launching region where the gas is too hot to produce optical lines.

Recent observations of broad band X-ray spectra of ULXs^{42,43,44} reveal that they have spectral cutoffs at relatively low energies (around ten keV), which are not seen in the spectra of sub-Eddington black hole binaries in the low/hard or high/soft states⁴⁵. Thus, the physical conditions of the innermost disc are indeed quite different between

ULXs and sub-Eddington black hole binaries. The spectral cutoff in ULXs may be interpreted as indication of the supercritical accretion⁴⁶ (the "ultraluminous state"), where a massive wind may completely envelope the inner-disc regions, creating a cool Comptonizing photosphere. The broadband X-ray observations together with the optical observations presented here strongly support the picture for ULXs as supercritical discs.

One of the appreciable properties of some ULXs is quasi-periodic oscillations (QPOs) with periods of typically tens of seconds¹. The QPOs are stronger in hard X-ray bands. Remarkable modulations of the disc luminosity and the accretion rate through the inner edge of the disc were found⁴⁷ in time-dependent two-dimensional radiation hydrodynamical calculations performed for a supercritical accretion disc by adopting the parameters of SS 433. These modulations produce recurrent hot blobs in the SCAD funnel to become apparent as high amplitude QPOs. A time scale of the QPOs⁴⁷ is in about the same range as those observed in the ULXs.

Thus, we interpret that all these ULXs with X-ray luminosities of $L_x \sim 10^{40}$ erg s⁻¹ constitute a homogeneous class of stellar-mass black holes with supercritical discs. They are distinct population from hyperluminous X-ray sources (HLXs), which are most probably IMBHs⁴⁸.

References

28. Kashikawa, N. *et al.* FOCAS: The Faint Object Camera and Spectrograph for the Subaru Telescope. *Publ. Astron. Soc. Jap.* **54**, 819-832 (2002)
29. Kaaret, P., Ward, M. J. & Zezas, A. High-resolution imaging of the HeII $\lambda 4686$ emission line nebula associated with the ultraluminous X-ray source in Holmberg II. *Mon. Not. R. Astr. Soc.* **351**, L83-L88 (2004)
30. Ramsey, C. J. *et al.* An Optical Study of Stellar and Interstellar Environments of Seven Luminous and Ultraluminous X-Ray Sources. *Astrophys. J.* **641**, 241-251 (2006)
31. Soria, R., Cropper, M., Pakull, M., Mushotzky, R. & Wu, K. The star-forming environment of an ultraluminous X-ray source in NGC 4559: an optical study. *Mon. Not. R. Astr. Soc.* **356**, 12-28 (2005)
32. Liu, J.-F., Bregman, J. N. & Seitzer, P. The Optical Counterpart of an Ultraluminous X-Ray Source in NGC 5204. *Astrophys. J.* **602**, 249-256 (2004)
33. Grisé, F., Kaaret, P., Pakull, M. W. & Motch, C. Optical Properties of the Ultraluminous X-Ray Source Holmberg IX X-1 and Its Stellar Environment. *Astroph. J.* **734**, id. 23 (2011)
34. Cseh, D., Grisé, F., Corbel, S. & Kaaret, P. Broad Components in Optical Emission Lines from the Ultra-luminous X-ray Source NGC 5408 X-1. *Astroph.*

J. **728**, id. L5 (2011)

35. Liu, J., Orosz, J. & Bregman, J. N. Dynamical Mass Constraints on the Ultraluminous X-Ray Source NGC 1313 X-2. *Astrophys. J.* **745**, id. 89 (2012)

36. Crowther, P. A. et al. NGC 300 X-1 is a Wolf-Rayet/black hole binary. *Mon. Not. R. Astr. Soc.* **403**, L41-L45 (2010)

37. Silverman, J. M. & Filippenko, A. V. On IC 10 X-1, the Most Massive Known Stellar-Mass Black Hole. *Astrophys. J.* **678**, L17-L20 (2008)

38. van Kerkwijk, M. H., Geballe, T. R., King, D. L., van der Klis, M. & van Paradijs, J. The Wolf-Rayet counterpart of Cygnus X-3. *Astron. Astrophys.* **314**, 521-540 (1996)

39. Gräfener, G. & Hamann, W.-R. Mass loss from late-type WN stars and its Z-dependence. Very massive stars approaching the Eddington limit. *Astron. Astrophys.* **482**, 945-960 (2008)

40. Medvedev, P. S., Fabrika S. N., Vasiliev V. V., Goranskij V. P. & Barsukova E. A. Superbroad component in emission lines of SS 433. *Astronomy Letters* **39**, 826-843, (2013)

41. Ohsuga, K., Mori M., Nakamoto T. & Mineshige S. Supercritical Accretion Flows around Black Holes: Two-dimensional, Radiation Pressure-dominated Disks with Photon Trapping. *Astrophys. J.*, **628**, 368–381 (2005)

42. Bachetti, M. et al. The Ultraluminous X-Ray Sources NGC 1313 X-1 and X-2: A Broadband Study with NuSTAR and XMM-Newton. *Astrophys. J.* **778**, id. 163 (2013)

43. Walton, D. J. et al. Broadband X-Ray Spectra of the Ultraluminous X-Ray Source Holmberg IX X-1 Observed with NuSTAR, XMM-Newton, and Suzaku. *Astrophys. J.* **793**, id. 21 (2014)

44. Rana, V. et al. The Broadband XMM-Newton and NuSTAR X-Ray Spectra of Two Ultraluminous X-Ray Sources in the Galaxy IC 342. *Astrophys. J.* **799**, id. 121 (2015)

45. Done, C., Gierliski, M. & Kubota, A. Modelling the behaviour of accretion flows in X-ray binaries. Everything you always wanted to know about accretion but were afraid to ask. *A&ARv* **15**, 1-66 (2007)

46. Gladstone J. C., Roberts T. P. & Done C. The ultraluminous state. *Mon. Not. R. Astr. Soc.* **397**, 1836-1851 (2009)

47. Okuda, T., Lipunova, G. V. & Molteni, D. The jets and disk of SS 433 at super-Eddington luminosities. *Mon. Not. R. Astr. Soc.* **398**, 1668-1677 (2009)
48. Farrell, S. A., Webb, N. A., Barret, D., Godet, O. & Rodrigues, J. M. An intermediate-mass black hole of over 500 solar masses in the galaxy ESO243-49. *Nature* **460**, 73-75 (2009)

Supplementary Figure 1: Calibrated spectra of the ULX optical counterparts.

From top to bottom: the ULX in Holmberg II, Holmberg IX, NGC 4559, and NGC 5204. The two upper spectra were obtained on February 28, while the rest are the summed spectra from the three nights. For better visualization we add flux offsets of 1.8, 1.2 and 0.6 (10^{-17} erg/cm²s Å) for the Holmberg II, Holmberg IX, and NGC 4559 ULXs, respectively. Besides obvious hydrogen lines we mark He II lines ($\lambda 4686$ and $\lambda 5412$) and He I lines ($\lambda 5876$ and $\lambda 6678$), thick bar indicates position of the Bowen blend C III/N III $\lambda\lambda 4640 - 4650$.

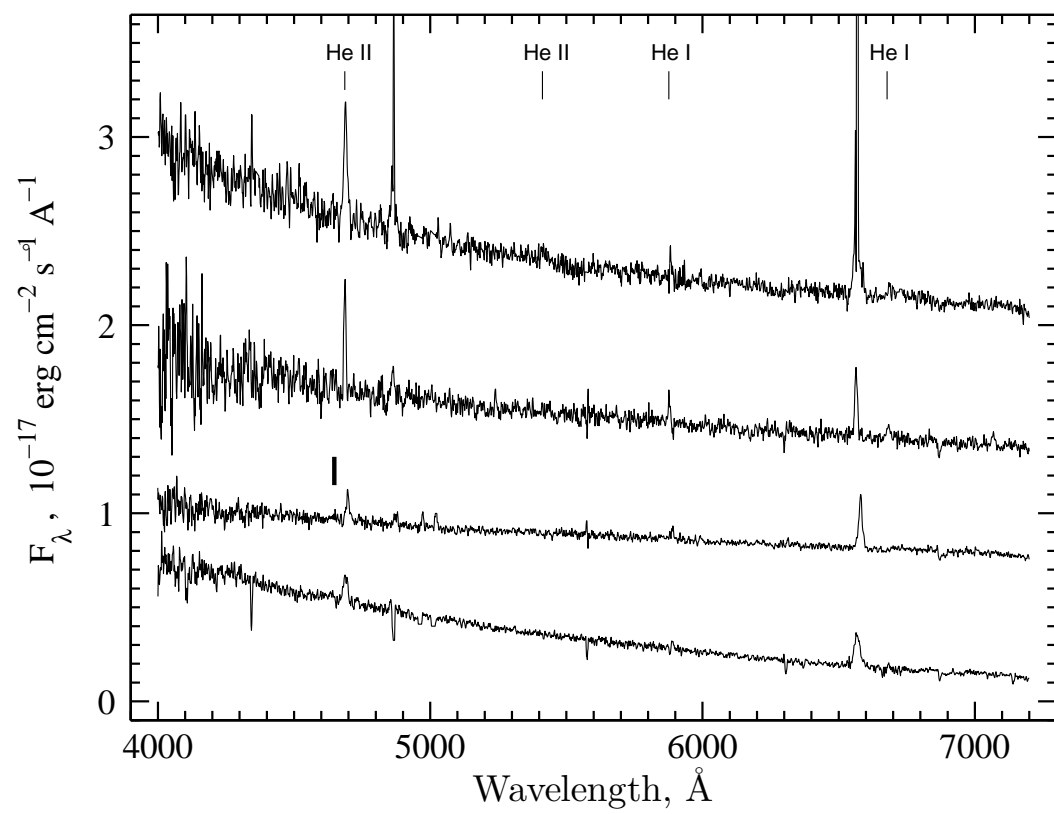
Supplementary Figure 2: Classification diagram of WNL stars in the LMC and our Galaxy⁷.

The black open squares, triangles, and circles mark WN 8, WN 9–10m, and WN 11 stars, respectively. The blue filled circle denotes ζ Pup. Other Galactic and LMC stars⁹ are O2If and O3If (open blue circles), O2If/WN5, O2.5If/WN6, O3If/WN6, and O3.5If/WN7 (blue crosses), and WN6ha and WN7ha stars (open blue squares). There are three known LBV – WNL transitions (AG Car, V 532, and HD 5980) in this diagram⁸. Consequent states of each LBV star are connected with the lines. Positions of our four ULX counterparts are also shown (connected with lines to show variability from night to night), together with those of SS 433, NGC 7793 P13, NGC 5408 X-1, NGC 1313 X-2, M 101 ULX-1, NGC 300 X-1, and IC 10 X-1^{10,14,15,16,18,36,37}.

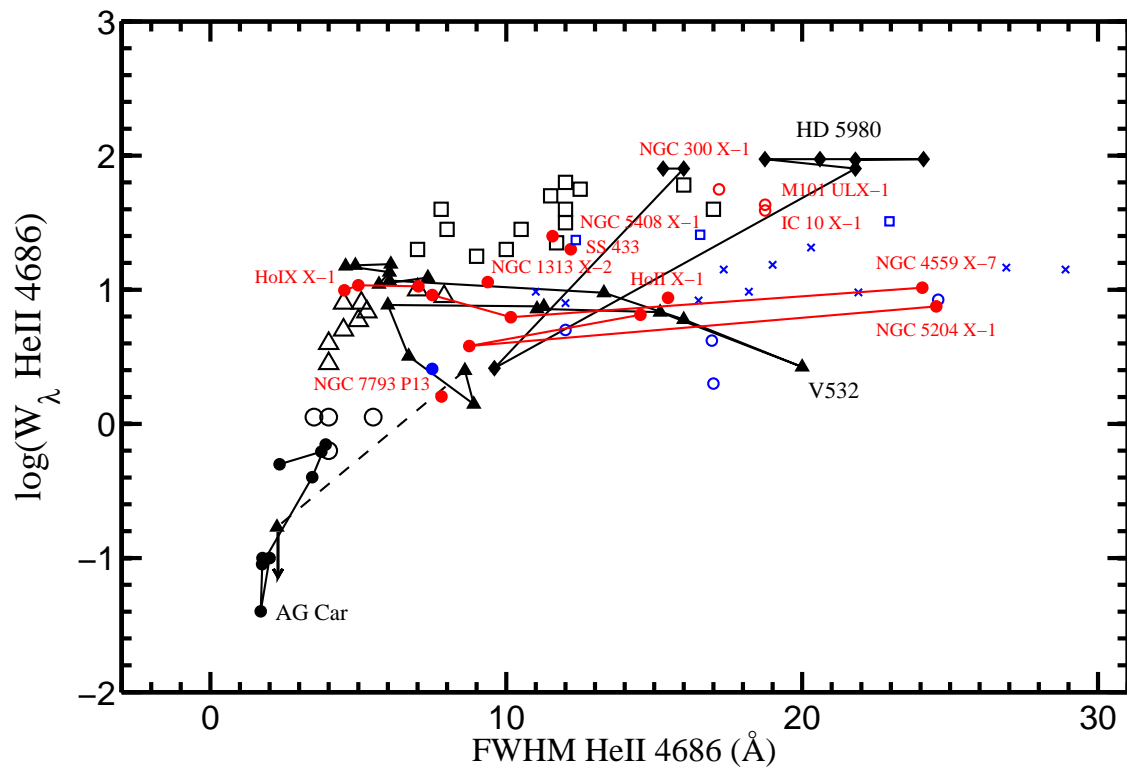
Supplementary Figure 3: Radial velocities of He II (blue) and H α (red) lines for three consequent nights.

From top to bottom: the ULX in NGC 4559, NGC 5204, and Holmberg IX. For the last target we show only the He II velocities (shifted by -300 km s⁻¹ from those of H α). To estimate the error in the radial velocity, we produced simulated spectra of the He II (or H α) line with the same profile (modelled by a Gaussian) and random noises as those of the real data. We regard the scatter (1σ) of their best-fit radial velocities as the error, which is attached to each data point.

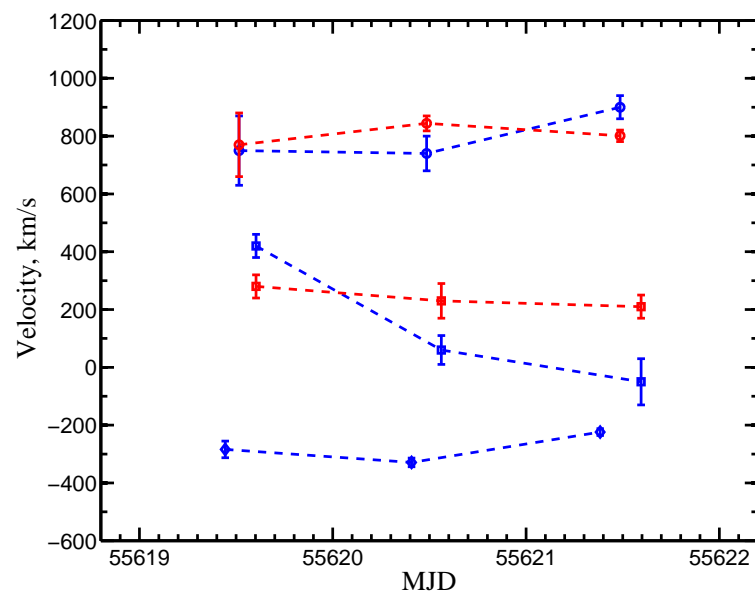
Supplementary Table 1: Mean emission line equivalent widths (in Angstroms) and their ratios of the main emission lines of our ULXs sample and SS 433. The data of SS 433 are taken from the literature^{10,24}. The last column presents the ULX equivalent widths and the line ratios with respect to those in SS 433.



Supplementary Figure 1 :



Supplementary Figure 2 :



Supplementary Figure 3 :

Supplementary Table 1 :

	EW_{ULX}	$EW_{SS\ 433}$	ULX / SS 433
He II $\lambda 4686$	9.0 ± 0.6	20	0.45 ± 0.03
He II $\lambda 5412$	$\lesssim 1.1 \pm 0.3$	2.5	$\lesssim 0.44 \pm 0.12$
He I $\lambda 5876$	$\lesssim 2.5 \pm 0.7$	24.5	$\lesssim 0.10 \pm 0.03$
H β	4.1 ± 1.2	50	0.082 ± 0.024
H α	25 ± 4	320 ± 20	0.078 ± 0.012
H β /H α	0.16 ± 0.06	0.16	1.0 ± 0.4
He II $\lambda 4686$ /H α	0.36 ± 0.06	0.06	6.0 ± 1.0
He I $\lambda 5876$ /H α	$\lesssim 0.10 \pm 0.03$	0.08	$\lesssim 1.3 \pm 0.4$